Using satellite data for mapping offshore wind resources and wakes

Charlotte Bay Hasager, Merete Bruun Christiansen, Morten Nielsen, Rebecca Barthelmie

Risoe National Laboratory, Wind Energy Department, Denmark

Abstract

Satellite Earth observing technology map ocean wind fields. The Synthetic Aperture Radar (SAR) technique of mapping ocean winds is based on the normalized radar cross-section backscattered values observed at the satellite. These data are a non-linear function of wind through the wind-generated capillarity waves at the ocean surface. SAR provides the highest spatial detail possible from satellite. SAR images have been used for two wind energy applications: offshore wind resource estimation and offshore wind farm wake quantification. For wind resource estimation, a tool is developed for applied use. Resulting maps on mean wind speed, Weibull A and k and uncertainty estimates are calculated. Results are presented for a series of ERS SAR images at Horns Rev in the North Sea with a grid cell resolution of 400 m by 400 m. The maps show spatial gradients in all parameters within the near-coastal zone. Preliminary maps covering Denmark are also presented with a resolution of 1.6 km by 1.6 km. These maps outline larger scale spatial variations in wind speed parameters. For offshore wake identification and quantification, high-resolution satellite SAR images are used both for the Horns Rev and Nysted wind farms. The results indicate wake velocity deficit downstream of the wind farms. The velocity deficit is dependent upon atmospheric stability with quicker recovery for unstable than near-neutral conditions. Airborne SAR images have also been analysed at Horns Rev and velocity deficit is identified with greater spatial detail than from satellite SAR.

Introduction

Satellite and airborne images recorded by Synthetic Aperture Radar are used for wind resource estimation offshore and for the study of wake downwind of large offshore wind farms. It is attractive to study and use satellite wind maps as the spatial details are recorded. The absolute accuracy is around 1 ms^{-1} for each wind speed map, yet the relative uncertainty within each map is far less, ~ 0.5 ms^{-1}. The relative uncertainty is related to the averaging of a number of grid cells. The more cells are averaged, the smaller the uncertainty. Though it is a balance to keep the spatial information intact, in order to quantify e.g. spatial gradients in wind speed at a scale that is relevant in wind turbine engineering.

Methodology

SAR images are calculated into wind speed using CMOD-4 developed by (Stoffelen and Anderson, 1997). Wind direction is found from analysis of streak directions in the images in a previous step. Hence the wind direction is input to CMOD-4 together with the calibrated and normalized backscatter values in the maps. For further information on the methodology, see e.g. (Hasager et al., 2004). The resulting maps show wind speed and wind direction. It is series of such mapped wind vector information that subsequently is used for assessing offshore wind resource and wind farm wake effects. The wind speed is valid at 10 m above sea level.

Data

SAR images are available from various satellites. In the present study we present the results based on the following data set:

- 30 ERS-2 SAR satellite images from Horns Rev in the North Sea
- 26 Envisat ASAR WSM satellite images from Denmark
- 19 ERS-2 SAR and Envisat ASAR APP and IMG satellite images from Horns Rev and Nysted wind farms
- Airborne SAR from the E-SAR flown by German Aerospace Centre (DLR) from Horns Rev wind farm

Results wind resource mapping

ERS-2 SAR satellite images

At Horns Rev in the North Sea a mean wind speed map is calculated based on 30 ERS-2 SAR satellite images. For the calculation the newly developed software RWT (Risoe Wemsar Tool) is used (Nielsen et al., 2004). Each wind speed map is in a resolution of 400 m by 400 m. This ensures much spatial detail to be quantified. In fig. 1 the mean wind speed map is graphed.

It is only within the area outlined with a black line that all 30 images cover. Hence the statistics within this area can be interpreted. This area covers both the present wind farm and the prospected new wind farm. Both wind farms cover areas around 4 km by 5 km. It is that the mean wind speed at 10 m above sea level is higher at the prospected area (western location) than at the present (eastern location).

The average mean wind speed along the horizontal transect from East to West is plotted in fig. 2. The transect starts 10 km from the shoreline and reaches 50 km offshore. It is clear that the mean wind speed increases offshore. Other results from RWT based on 30 satellite maps are Weibull A and k maps. In figure 2 the variation along the horizontal transect in both these parameters is shown.

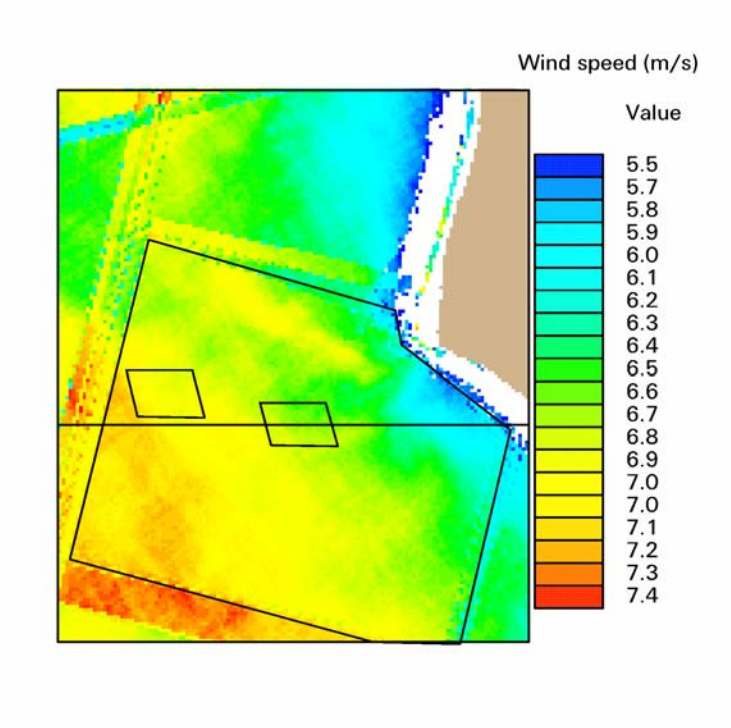

Fig. 1. Mean wind speed map based on 30 wind maps. The location of the present (eastern) and prospected (western) wind farm and the horizontal transect line is indicated (see figure 2 for the results along the horizontal transect).

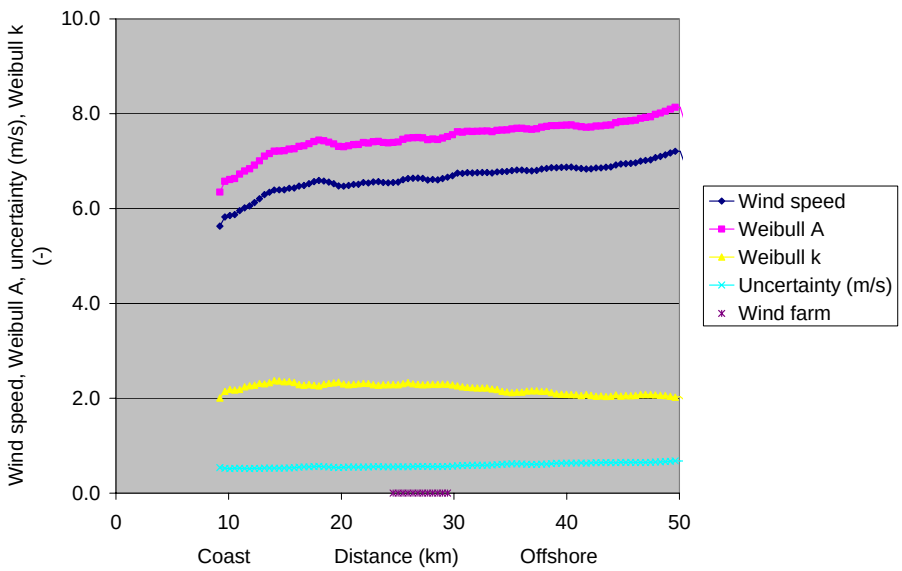

Fig 2. Wind statistics along a horizontal transect line from the coast and through the Horns Rev wind farm based on 30 wind maps from ERS SAR collected prior to construction of the wind farm. The wind farm is located 25 to 30 km offshore (indicated with a short purple line).

Envisat ASAR WSM satellite images

The Envisat ASAR satellite sensor is possible to program to ~ 35 different modes. One of these is the WSM mode: wide swath mode, in which the SAR scans a 400 km swath along the flight track. This is in contrast to e.g. ERS-2 SAR described above that only has one mode namely a 100 km swath. Hence from ERS all images cover areas of 100 km by 100 km. From Envisat we can obtain images of 400 km by 400 km. The larger coverage on the one hand is good for getting more area mapped in one snapshot, yet on the other hand the spatial detail is reduced a factor 4. The grid cells in the wind maps are 1.6 km by 1.6 km in Envisat ASAR WSM wind speed maps.

CMOD-4 is applied to the Envisat ASAR WSM images using the Johns Hopkins University, Applied Physics Laboratory (JHU, APL) software for analysis. An example of a wind speed map using the option of wind direction from the NOGAPS meteorological model is shown in Figure 3. Further information on the JHU/APL method is given in (Monaldo, 2000;Monaldo et al., 2001;Thompson et al., 2001;Monaldo et al., 2003)

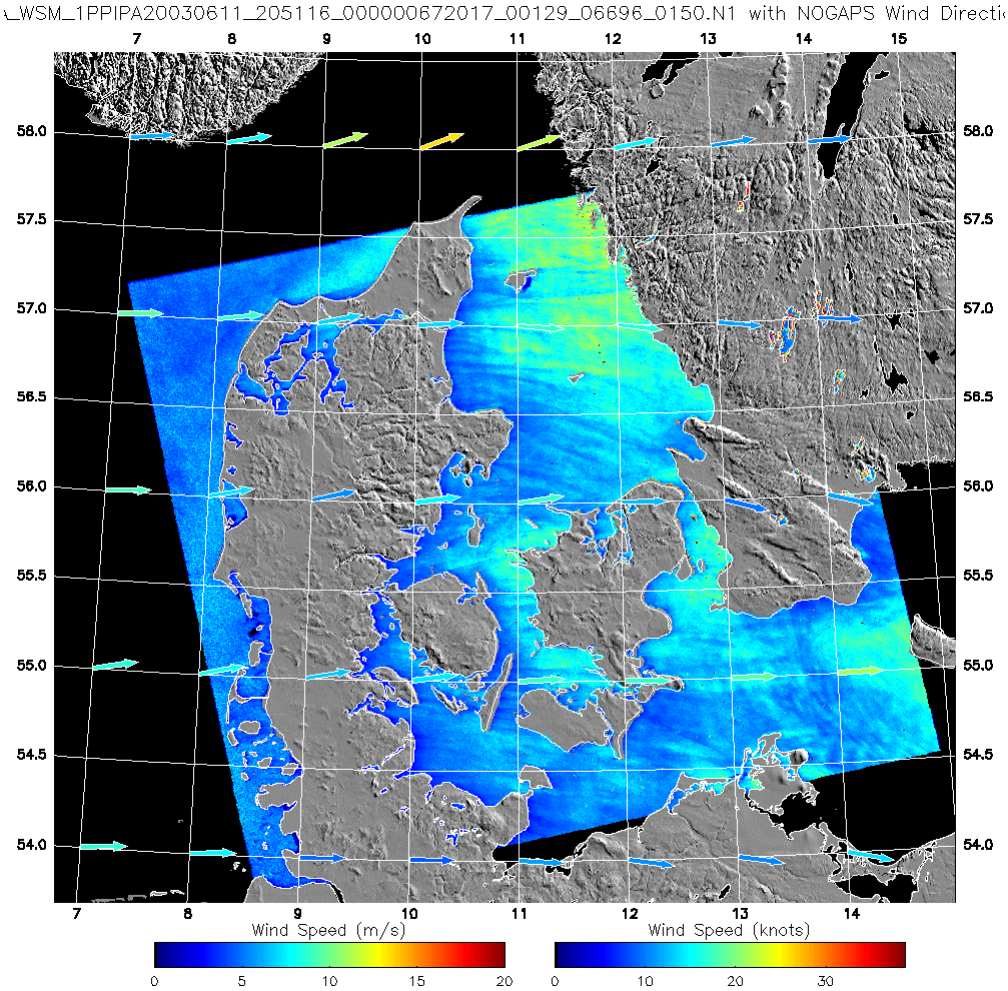

Fig. 3 Envisat ASAR wide-swath wind map from JHU/APL (Merete B. Christiansen) from June 11th, 2003. It is the NOGAPS model wind directions used in CMOD-4.

A series of 26 Envisat ASAR WSM wind vector maps are used in RWT software. An example of statistics is given in figure 4. Based on only 5 satellite images a preliminary resulting map is found. The work is in progress to include 26 images.

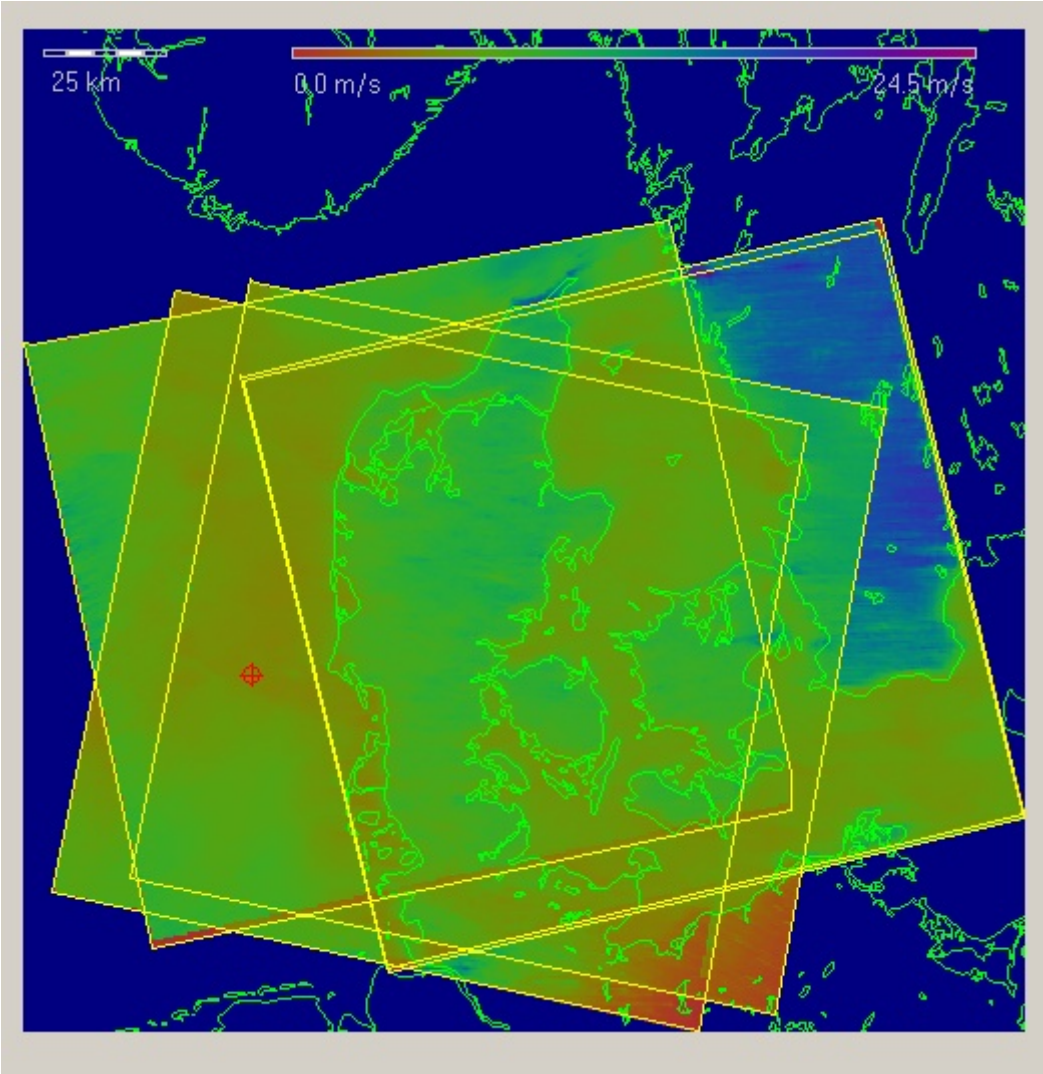

Figure 4. Mean wind speed map based on 5 Envisat ASAR WSM satellite images covering Denmark. The yellow pologones outline each image, hence only in the central area all 5 images are available and the statistics are useful for spatial interpretation.

Results on offshore wind farm wake studies

Offshore wind farms typically are located in large arrays such that sharing grid connection is feasible. Also sea bottom topography may determine the outlay of wind farms offshore.

The effect of offshore wind farms on the average mean wind speed and turbulence is investigated using satellite image data. Around 45 high-resolution satellite images from ERS-2 and Envisat were obtained. It soon showed, however, that the sea bottom topography, rain effects and other issues, provide noise effects visible in the wind maps. Therefore the full analysis on wake velocity deficit was performed on only 19 image covering both the Horns Rev and Nysted wind farms. Full reporting is provided in (Christiansen and Hasager, 2005a).

One example on the reduction in mean wind speed is shown in figure 5. In the horizontal transect 1 the transect passes far from the wind farm and aligned with the wind direction. The second transect passes through the wind farm aligned with the wind direction. It is clear that the wind speed in the undisturbed flow in transect 1 is nearly constant whereas transect 2 through the wind farm experienced a reduced mean wind speed just after the wind farm.

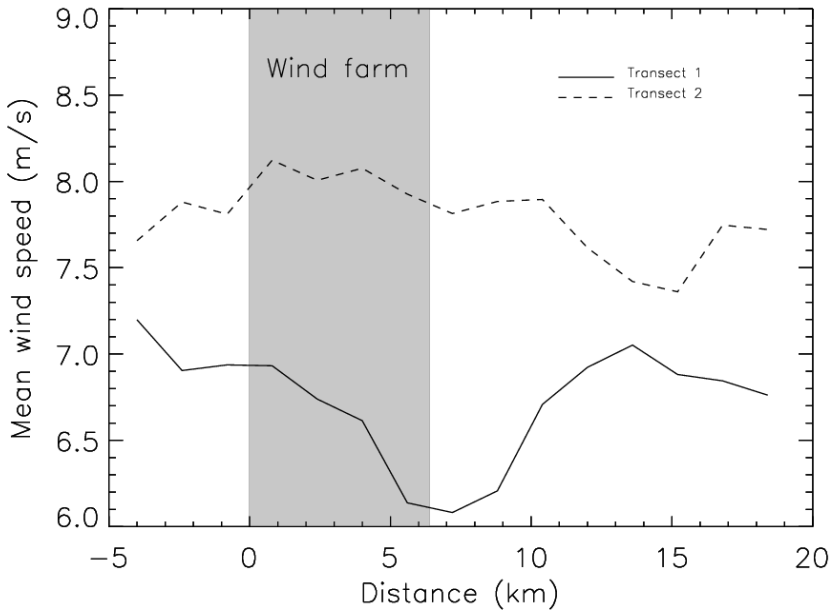

Fig. 5. Wind speed from ERS-2 SAR satellite wind map from March 01, 2003. Two horizontal transects are shown: Transect 1: through wind farm (which is outline in grey shading); Transect 2: non-obstructed reference transect, displaced 8 km from transect 1. From Monaldo et al. 2005.

Airborne SAR wind maps

On 12 October 2003 the aircraft from the German Aerospace Centre (DLR) flew with a SAR near Horns Rev wind farm. Fig. 6 shows the outlay of the flight tracks. The wind was ~ 10 ms^{-1} from NNW. During the campaign the wind speed decreased. Short tracks across the wake region downwind of the wind farms (S1, S2 and S3) as well as long tracks aligned with the wind (L1 and L2) were obtained.

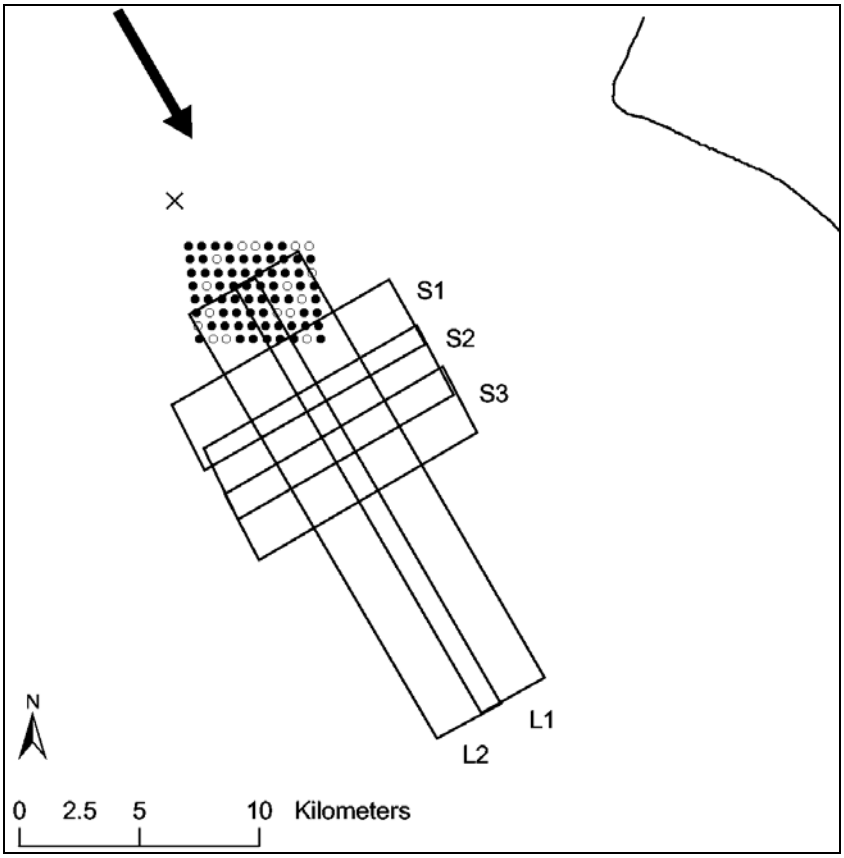

Fig. 6. Horns Rev wind farm with E-SAR airborne flight tracks indicated. Configuration of E-SAR flight tracks acquired in C-band VV. Arrow indicates wind direction (330º), x the meteorological mast and dots are wind turbines (filled if running). From (Christiansen and Hasager, 2005b)

Results

In the short tracks the wake is observed near the wind farm and free stream wind speed is found just outside the wind farm. When knowing the free stream velocity it is possible to calculate the velocity deficit, $VD=(U_{ref}-U)/U_{ref}*100\%$, where U is the wind observed in the wake and U_{ref} is the free stream wind. Two resulting figures are shown below. Figure 7a contains the velocity deficit in S1, S2 and S3 separately, and Figure 7b shows the average velocity deficit for the three transects.

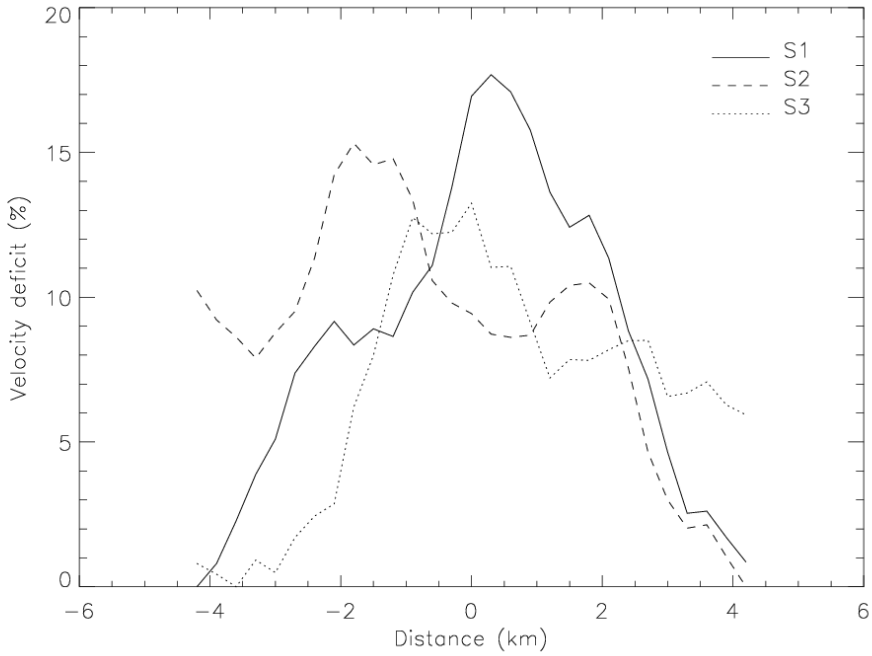

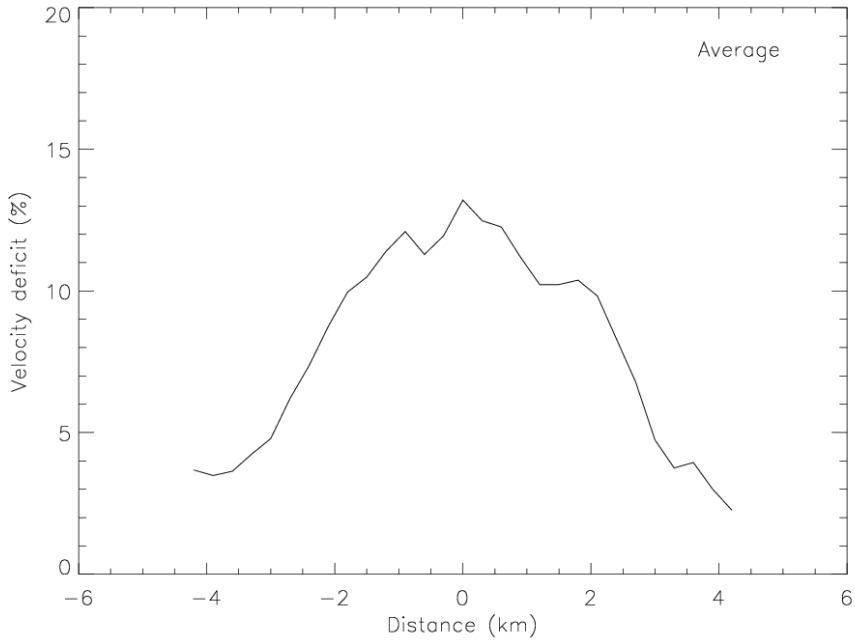

Fig. 7 a) Velocity deficit obtained for short E-SAR tracks (S1-S3). Distances of 0 km are downstream of wind farm centre. b) average of the three transects in a).

From figure 7a it is clear that the maximum velocity deficit observed is around 18% in the horizontal transect (s1) closer to the wind farm. The maximum deficit in the two transect (S2 and S3) further from the wind farm the maximum velocity deficits are 16% and 14 %, respectively. It is also clear that the maximum velocity deficit is moving about 1 to 2 km from the centreline aligned with the wind direction. The wind direction is nearly constant, hence the results may indicate a type a meandering of the wake. The tracks were recorded at S1 at 9.28-9.30, S2 at 10.06-10.08 and S3 at 10.18-10.20 Danish standard time on 12 October 2003. The wind direction at 28 m the meteorological mast at the three occasions were 332º, 317º and 316º, respectively, and the wind speed 10.8 ms^{-1}, 9.3 ms^{-1} and 8.6 ms^{-1}. It is important to normalize the wind speed map with a proper free stream wind speed as the wind was not stationary through the complete flight campaign that lasted from 8.35 to 11.30 and include several more flight tracks. A full reporting is in progress. Figure 8 shows the aircraft in Esbjerg Airport prior to flight.

Figure 8. The DLR aircraft in Esbjerg Airprot 12 October 2003. It carries a C-band and L-band polarimetric SAR.

Conclusion

Satellite and airborne SAR wind maps reveal variations in winds speed relevant for wind engineering. Wind resource mapping is not accurate in a stand-alone mode, yet may prove useful in feasibility studies. Wake effects quantified spatially from satellite and aircraft compare well to other observations and model results. For applied use the RWT software is available for wind engineers.

Acknowledgements

Satellite SAR images are provided by the European Space Agency (ESA) EO-1356 project. Funding for satellite and aircraft SAR data was provided by STVF at the Danish Research Council for the SAR-WAKE project. Funding for the national wind

resource study was provided by STVE in the SAT-WIND project. Development of software is partly funded by EU-WEMSAR project and ESA EOMD EO-Windfarm projects in collaboration the Nansen Environmental and Remote Sensing Centre (NERSC) in Norway. Johns Hopkins University, Applied Physics Lab. we acknowledge the use of software for calculation of wind maps from Envisat ASAR WSM. Meteorological data from Elsam Engineering.

References Cited

Christiansen, M. B., and C. B. Hasager, 2005a, Wake effects of large offshore wind farms identified from satellite SAR: Remote Sensing of Environment.

Christiansen,MB, C B Hasager. Wake studies around a large offshore wind farm using satellite and airborne SAR. 2005b. Skt. Petersburg, Russia, 20-24 June 2005. 31st International Symposium on Remote Sensing of Environment (ISRSE).
Ref Type: Conference Proceeding, cd-rom

Hasager, C. B., E. Dellwik, M. Nielsen, and B. Furevik, 2004, Validation of ERS-2 SAR offshore wind-speed maps in the North Sea: International Journal of Remote Sensing, v. 25, no. 19, p. 3817-3841.

Monaldo, F., 2000, The Alaska SAR demonstration and near-real-time synthetic aperture radar winds: John Hopkins APL Technical Digest, v. 21, p. 75-79.

Monaldo,F, V Kerbaol, P Clemente-Colón, B Furevik, J Horstmann, J Johannessen, X Li, W Pichel, T D Sikora, D J Thomson, C Wackerman. The SAR measurement of ocean surface winds:an overview. ESA SP-565, 15-32. 2003. ESA. Proceedings of the Second Workshop Coastal and Marine Applications of SAR, 2-12 September 2003, Svalbard, Norway.
Ref Type: Conference Proceeding

Monaldo, F. M., D. R. Thompson, R. C. Beal, W. G. Pichel, and P. Clemente-Colón, 2001, Comparison of SAR-derived wind speed with model predictions and ocean byou measurements: IEEE Transactions on Geoscience and Remote Sensing.

Monaldo, F.M.; Thompson, D.R.; Winstead, N.S.; Pichel, W.G.; Clemente-Colón, P., Christiansen, M.B., High-resolution wind field measurement from synthetic aperture radar and its application to the measurement of barrier jets and wind power production. Johns Hopkins APL Technical Digest, in press.

Nielsen,M, P Astrup, C B Hasager, R J Barthelmie, S C Pryor. Satellite information for wind energy applications. Risø-R-1479(EN), 1-57. 2004. Roskilde, Denmark, Risø National Laboratory.
Ref Type: Report

Stoffelen, A., and D. L. T. Anderson, 1997, Scatterometer data interpretation: Estimation and validation of the transfer fuction CMOD4: Journal of Geophysical Research, v. 102, no. C3, p. 5767-5780.

Thompson, D. R., F. M. Monaldo, R. C. Beal, N. S. Winstead, W. G. Pichel, and P. Clemente-Colón, 2001, Combined estimates improve high-resolution coastal wind mapping: EOS, Transactions, American Geophysical Union, v. 82, no. 41, p. 1-3.